



Ages of Large Magellanic Cloud Star Clusters with Gemini Multi-Object Spectrograph Integrated Spectroscopy: Systematic Comparison of Available Tools

Martina I. Tapia-Reina^{1,2,3} , Randa Asa'd⁴ , Andrea V. Ahumada^{1,2} , and Carlos Gonzalo Díaz^{1,2}

¹ Universidad Nacional de Córdoba, Observatorio Astronómico de Córdoba, Laprida 854, X5000BGR, Córdoba, Argentina

² Consejo Nacional de Investigaciones Científicas y Técnicas (CONICET), Godoy Cruz 2290, C1425FQB, Buenos Aires, Argentina

³ Universidad Nacional de Córdoba, Facultad de Matemática, Astronomía, Física y Computación (FAMAF), Córdoba, Argentina

⁴ Physics Department, American University of Sharjah, P.O. Box 26666, Sharjah, UAE

Received 2025 March 7; revised 2025 June 20; accepted 2025 June 20; published 2025 July 16

Abstract

We present the first systematic analysis comparing the ages, reddening, and radial velocities of star clusters using two widely used tools: STARLIGHT and Analyzer of Spectra for Age Determination (A.S.A.D). Both tools utilize the full integrated spectrum fitting technique but they use different approaches in calculating the parameters. We find that there is a good agreement between the parameters derived by the two tools and confirm that both tools provide consistent results with the literature parameters obtained from resolved photometry. We note that for optimal age and reddening estimates, observed integrated spectra should have signal-to-noise ratio (S/N) > 10 when using A.S.A.D and the combination of the single stellar populations should be added linearly (not using logarithmic values) when using STARLIGHT. We also show that the deviation of the radial velocity estimates between the two tools depends on the S/N of the observed integrated spectrum and demonstrate that when varying the metallicity, the age estimates of STARLIGHT are not affected significantly, while the results of A.S.A.D are generally underestimated. As more observational data become available through modern instruments, the strengths and limitations of each available automated tool need to be taken in consideration when interpreting their results.

Unified Astronomy Thesaurus concepts: [Star clusters \(1567\)](#); [Spectroscopy \(1558\)](#); [Magellanic Clouds \(990\)](#)

1. Introduction

Star clusters stand as a pivotal yardstick in modern astrophysics. They are excellent targets to determine stellar ages and metallicities providing rich information on the star formation and chemical histories of their host galaxies (e.g., L. Greggio & A. Renzini 2011; A. Adamo et al. 2020; S. C. Berek et al. 2023). Ages, metallicities, radial velocities, and reddening of star clusters can be obtained using the integrated spectrum fitting technique both in the Local Group and in more distant galaxies (e.g., T. H. Puzia et al. 2005, 2006; R. P. Schiavon et al. 2005; J. F. C. Santos et al. 2006; T. Palma et al. 2008; R. Cid Fernandes & R. M. González Delgado 2010; J. E. Colucci et al. 2012, 2017; R. S. Asa'd et al. 2013; J. Clariá et al. 2017; I. V. Chilingarian & R. Asa'd 2018; A. V. Ahumada et al. 2019; N. Bastian et al. 2019; T. C. Moura et al. 2019; C. M. Sakari et al. 2021; F. Simondi-Romero et al. 2022). Several automated tools have been developed to apply this powerful technique in the optical range and they are widely used in the literature. STARLIGHT (R. Cid Fernandes et al. 2005), NBursts (I. Chilingarian et al. 2007), EZ_{age} (G. J. Graves & R. P. Schiavon 2008), FISA (A. Benítez-Llambay et al. 2012), and Analyzer of Spectra for Age Determination (A.S.A.D; R. S. Asa'd 2014) are some examples.

The precision of some of these tools has been examined in detail. G. Gonçalves et al. (2020) analyzed the precision of the parameters obtained using STARLIGHT for different wavelength ranges within the optical regime. R. Asa'd & P. Goudfrooij (2020) investigated the precision of the ages and metallicities of

21,000 mock simple stellar populations in the optical range using A.S.A.D. The influence of the stellar cluster mass on the precision of the age determination was studied in P. Goudfrooij & R. S. Asa'd (2021) from the blue optical through the mid-infrared and the precision of deriving possible age spreads within a star cluster using 118,800 mock star clusters has been discussed in R. Asa'd et al. (2021). R. Asa'd et al. (2022) presented the first systematic analysis comparing the age, metallicity, and reddening of star clusters from resolved versus unresolved data using the same sets of isochrones. However, despite the steps taken to investigate the precision of each tool separately, there has not been a systematic comparison between the parameters obtained from the different tools using the same observations and the same models. The aim of this work is to fill this gap by performing a systematic comparison between ages, reddening and radial velocities obtained from STARLIGHT and A.S.A.D using a new sample of 12 star clusters in Large Magellanic Clouds (LMCs) observed with the Gemini Multi-Object Spectrograph at Gemini South (GMOS-S). This is much needed because the ages obtained from the full spectrum fitting technique using different tools often differ, although all use the χ^2 minimization method. This is due to the details of the approach of each tool (as explained in 4). This can lead to different ages for a star cluster using the same observed integrated spectrum and the same model. Investigating how significant this difference helps to highlight the strengths and limitations of each tool.

In Section 2 we provide details about our new observations and the data reduction process. In Section 3 we present the models used and in Section 4 we highlight the methods applied by STARLIGHT and A.S.A.D to provide the ages, reddening, and radial velocities. The results are discussed in Section 5 and the summary of our work is given in Section 6.



Original content from this work may be used under the terms of the [Creative Commons Attribution 4.0 licence](#). Any further distribution of this work must maintain attribution to the author(s) and the title of the work, journal citation and DOI.

Table 1
Exposure Time, S/N, Radial Velocity, Reddening, and Difference Values from Both Codes for Each Star Cluster

Cluster	Exposure ^a	S/N ^b	Radial Velocity			$E(B - V)$		
			(km s ⁻¹)			(mag)		
			STARLIGHT	A.S.A.D	ΔV_r	STARLIGHT	A.S.A.D	$\Delta E(B - V)$
NGC 1711	82 × 10 s	31	321.9 ^{+0.00} _{-217.39}	339.0 ^{+0.0} _{-0.0}	17.03	0.02 ± 0.00	0.02 ± 0.09[[0.00
NGC 1718	44 × 35 s	35	212.83 ^{+67.53} _{-3.86}	170.0 ^{+14.2} _{-10.3}	42.83	0.30 ± 0.01	0.22 ± 0.03	0.08
NGC 1801	32 × 35 s	26	194.35 ^{+3.17} _{-2.82}	176.0 ^{+7.9} _{-6.3}	18.35	0.030 ± 0.004	0.00 ^{+0.05} _{-0.02}	0.03
NGC 1806	58 × 10 s	11	335.57 ^{+150.00} _{-130.00}	237.0 ^{+11.5} _{-13.1}	98.57	0.29 ^{+0.04} _{-0.03}	0.50 ^{+0.02} _{-0.03}	0.21
NGC 1818	30 × 23 s	26	208.84 ^{+11.16} _{-2.67}	191.0 ^{+7.1} _{-8.1}	17.84	0.0500 ± 0.0002	0.24 ± 0.12	0.19
NGC 1849	14 × 134 s	36	241.14 ^{+12.24} _{-2.82}	192.0 ^{+2.4} _{-1.9}	49.14	0.140 ^{+0.004} _{-0.005}	0.07 ± 0.06	0.07
NGC 1866	22 × 36 s	40	260.43 ^{+125.39} _{-13.97}	257.0 ^{+0.0} _{-1.2}	3.43	0.120 ^{+0.007} _{-0.003}	0.06 ± 0.05	0.06
NGC 1916	22 × 7 s	31	228.01 ^{+13.71} _{-3.21}	177.0 ^{+4.8} _{-7.3}	51.01	0.01 ± 0.0	0.16 ± 0.11	0.15
SL 505	30 × 116 s	22	138.31 ^{+5.83} _{-6.07}	114.0 ^{+12.6} _{-14.6}	24.31	0.46 ± 0.02	0.36 ± 0.04	0.10
NGC 2100	22 × 36 s	30	188.23 ^{+2.67} _{-3.46}	177.0 ^{+7.8} _{-7.6}	11.23	0.170 ± 0.003	0.34 ^{+0.10} _{-0.08}	0.17
NGC 2136	34 × 30 s	20	297.50 ^{+239.04} _{-17.82}	338.0 ^{+0.0} _{-0.0}	40.50	0.00 ^{+0.01} _{-0.0}	0.00 ± 0.10	0.00
NGC 2137	34 × 30 s	16	270.05 ^{+0.00} _{-7.71}	333.0 ^{+0.0} _{-0.0}	62.95	0.00 ± 0.00	0.00 ± 0.09	0.00

Notes. Errors are also indicated for each parameter.

^a Total observation time is indicated as the number of slit positions and the corresponding exposure time in seconds.

^b S/N was measured in the (4500–4700) Å spectral range in the final spectra.

2. Observation and Data Reduction

We selected a sample of LMC star clusters that span a broad age range from $\log(\text{age yr}^{-1}) \sim 7.2$ to 10.0. The observations were carried out using Gemini facilities in semesters 2019A (GS-2019A-Q-402; PI: Andrea Ahumada), 2019B (GS-2019B-Q-401; PI: Andrea Ahumada), and 2021B (GS-2021B-Q-401; PI: Andrea Ahumada). The data were obtained using GMOS-S in longslit mode (slit length of 5.5) with the B600 (6001 mm⁻¹) grating in the wavelength range from 3500 Å to 6700 Å. The grating was centered at 5100 Å and 5200 Å to cover the CCD chip gaps. The slit width of 2'' provided a spectral resolution of ~ 10 Å and we selected a slit position angle that allowed us to use a suitable guide star for each observation. Appendix A Table provides the number of slit positions per target, along with the scanned width, slit position angle, parallactic angle, airmass, and the corresponding atmospheric differential refraction (ADR) values (estimated from Table 1 in A. V. Filippenko 1982). The final column reports the ADR-to-Scan width percentage—defined as the ADR offset relative to the scanned width—ranging from 0.9% to 3.8%, assuming a worst-case scenario where the slit is oriented 90° from the parallactic angle. We note that although ADR can alter the continuum shape when the slit is not aligned with the parallactic angle (A. V. Filippenko 1982), this effect is negligible in our case. Since all our observations have smaller angular offsets, the actual ADR impact is even lower. Moreover, any potential light loss would occur only at the edges of the scanned field, where stellar densities—and thus flux contributions—are significantly lower. The cluster cores, which dominate the integrated signal, are fully sampled by overlapping slit positions. Therefore, ADR has negligible effect on the final integrated spectra and does not significantly impact the shape of the continuum.

The exposure times, which depend on both the size and the brightness of the star cluster, and the signal-to-noise ratio (S/N) as measured in the final spectra are listed in Table 1. The total integration time of the observation was split into different exposures by making telescope offsets perpendicular to the slit in order for the central part of the star cluster to be fully scanned.

The data was reduced using PyRAF, which is a Python⁵ wrapper for IRAF,⁶ and the Gemini IRAF package. We also used our own script-driven pipeline on Python, following standard procedures. For each science spectrum, we obtained an arc and flat taken with each exposure and created a master bias and a master flat-field. We performed a bias subtraction from the science spectra and flats, then the science spectra were flat-field normalized. After that, we created our own bad pixel mask by visually inspecting each science image using the DS9 viewer. The wavelength calibration was determined from Cu-Ar lamp taken either before or after the science exposures. Cosmic rays were identified and removed following the method of P. G. van Dokkum (2001) with a detection limit of 4.0, a fractional detection limit for neighboring pixels of 0.35, a contrast limit of 1.5, and a maximum of five iterations. The spectra were then traced, background subtracted, and extracted. The standard star spectra were reduced in the same way, and it was used to trace the sensitivity function which was then applied to the cluster spectra.

The extraction of the region of interest for each cluster from the 2D image was conducted interactively using the Gemini IRAF tasks *gsextract*. The Figure from Appendix A shows the region included in the integrated spectrum of each cluster. Finally, we combined the spectra of the same star cluster using *scombine*. No specific weights were used in the combination because the exposure times of each observation were equal.

3. Models

We used G. Bruzual & S. Charlot (2003; hereafter BC03) models adopting Padova isochrones (P. Marigo et al. 2008) and G. Chabrier (2003) IMF for a grid of 23 simple stellar populations (SSPs) of different ages ranging from $\log(\text{age yr}^{-1}) = 6$ to 10.1 (1 and 13,000 Myr) and a fixed metallicity of $[\text{Fe}/\text{H}] = -0.37$ ($Z = 0.008$) representing the

⁵ <https://www.python.org/>

⁶ IRAF is distributed by the National Optical Astronomical Observatories, which are operated by the Association of Universities for Research in Astronomy, Inc., under cooperative agreement with the National Science Foundation.

LMC metallicity (S. Choudhury et al. 2016). We used the same grid with both STARLIGHT and A.S.A.D. We chose a fixed metallicity value for our analysis in order to minimize the parameter space for a more precise comparison between the results obtained from the two tools. We applied reddening correction using galactic extinction law from J. A. Cardelli et al. (1989; with $R_v = 3.1$), and normalized the observations and models at 4020 Å. We used the wavelength range from 3800 Å to 5000 Å, which has shown to give more accurate results in both STARLIGHT (G. Gonçalves et al. 2020) and A.S.A.D (R. Asa'd & P. Goudfrooij 2020).

4. Method

Both STARLIGHT and A.S.A.D analyze the integrated spectrum of a star cluster to estimate the age, reddening, and radial velocity; however, the two tools use different approaches. In this section, we provide details about the approach used by each tool.

4.1. STARLIGHT

STARLIGHT spectral synthesis (R. Cid Fernandes et al. 2005)⁷ is a Fortran 77 program that fits the observed spectrum O_λ with a model M_λ which adds up N_* SSPs from a predefined set of base spectra according to the equation:

$$M_\lambda = M_{\lambda_0} \left[\sum_{j=1}^{N_*} x_j b_{j,\lambda} r_\lambda \right] * G(\nu_*, \sigma_*) \quad (1)$$

where M_{λ_0} is the model flux at the normalized wavelength, N_* is the number of SSPs used, x_j ($j = 1, \dots, N_*$) are the contribution percentages of each SSP, $b_{j,\lambda} = L_j(\lambda)/L_j(\lambda_0)$ is the spectrum of the j th SSP normalized at λ_0 , $r_\lambda = 10^{-0.4(A_\lambda - A_{\lambda_0})}$, and $G(\nu_*, \sigma_*)$ is a Gaussian distribution centered at velocity ν_* and with a σ_* dispersion.

STARLIGHT provides the results of the best-fitting SSP mixture that matches the observed integrated spectrum along with the final synthetic spectrum, which represents the combined contributions of the different SSP population mixtures. The code also outputs the A_v value—used to compute $E(B - V)$ —and information on the radial velocity. These are built-in components that can not be isolated or excluded when performing the fitting. Although most stellar clusters are expected to follow a single SSP, multicomponent fits often arise due to contamination, limited resolution and many other causes (B. Dias et al. 2010) and R. Cid Fernandes & R. M. González Delgado (2010) shows the analysis of the SSP contributions can help assess the reliability of single-SSP solutions. We therefore adopted the weighted average age of those SSPs contributing more than 5% to the mixture. It is worth stressing that STARLIGHT does not provide uncertainties, which were calculated as described in Section 5.1.

4.2. A.S.A.D

A.S.A.D. is an interactive user-friendly Python 2.7 program that can predict the age, reddening and radial velocity of star clusters from their observed integrated spectra by comparing the observations to synthesis model spectra according to the

equation:

$$\chi^2 = \sum_{\lambda=\lambda_{\min}}^{\lambda_{\max}} \left[\frac{(O_\lambda - M_\lambda)^2}{O_\lambda} \right] \quad (2)$$

where O_λ is the observed flux and M_λ is the model flux in R. S. Asa'd (2014). Note that the model flux here corresponds to the single SSP from the base model, in contrast to the multicomponent mixture used in STARLIGHT.

A.S.A.D. allows the user to choose whether to include reddening and radial velocity in the analysis—an option we enabled in our work. The code constructs the unreddened and normalized spectrum for each available SSP model, and then performs a χ^2 minimization. The final parameters correspond to the selected SSP model that best matches the observations. The tool outputs the results for all clusters simultaneously and allows users to assess the fit quality through surface plots and residual spectra for each model-observation combination.

5. Results and Discussion

According to R. Cid Fernandes et al. (2005), R. Cid Fernandes & R. M. González Delgado (2010), the weighted average of the different SSP contributions is obtained by selecting and applying Equation (3) to calculate the age.

$$\overline{\log(t_w(\text{yr}))} = \frac{\sum_{j=1} x_j * \log(t_j(\text{yr}))}{\sum_{j=1} x_j} \quad (3)$$

where $x_j(\%)$ represents the percent contribution of the SSP with age t_j .

Figure 1 shows the SSP mixture obtained with STARLIGHT as well as the weighted average $\log(\text{age})$, ($\log(t_w(\text{yr}))$), and the \log of weighted average age, ($\log(\bar{t}_w(\text{yr}))$), for each cluster in our sample. The dominant SSP (90.6%) for NGC 1711 has $\log(\text{age yr}^{-1}) = 7.4$ (25 Myr) and the second SSP of $\log(\text{age yr}^{-1}) = 8.21$ has a contribution of only 9.4% to the best-fitting synthetic spectrum. The weighted average age for this cluster is $\log(t_w(\text{yr})) = 7.48$. A similar behavior is seen for NGC 1801 and NGC 2100 where two SSPs contribute to the age estimation of the cluster. NGC 1806 has a weighted average age of $\log(t_w(\text{yr})) = 9.51$ with contribution from three SSPs. Figure 1 shows that there is a 80.8% contribution of $\log(\text{age yr}^{-1}) = 9.63$ in addition to 13.9% of $\log(\text{age yr}^{-1}) = 8.96$ and 5.3% of $\log(\text{age yr}^{-1}) = 9.16$. Similar behavior is noticed for NGC 1818, NGC 1849, and NGC 1866. For NGC 1718, STARLIGHT combines six SSPs with the highest contribution of 43.4% for $\log(\text{age yr}^{-1}) = 8.71$ (512 Myr) and lowest contribution of 5.3% for $\log(\text{age yr}^{-1}) = 10$ (10 Gyr). There are two more clusters in our sample that show the same behavior of including more than three SSPs for ultimate age estimation: NGC 1916 with four SSPs and SL 505 with seven SSPs. With the exception of NGC 2136, most star clusters show one predominant SSP. See the Appendix B table for the details of SSPs contributions.

We developed a Python code that can apply Equation (3); however, the figure in Section Appendix C reveals that NGC 1718 and SL 505 for which STARLIGHT uses 6 and 7 combinations of SSP, respectively, are outliers as their age estimates are greater than 1σ from the unity line. When using the same equation with $\log(\bar{t}_w(\text{yr}))$ instead of $\log(t_w(\text{yr}))$, the correlation improves significantly. We show the results

⁷ Version 04, available from <http://www.starlight.ufsc.br>.

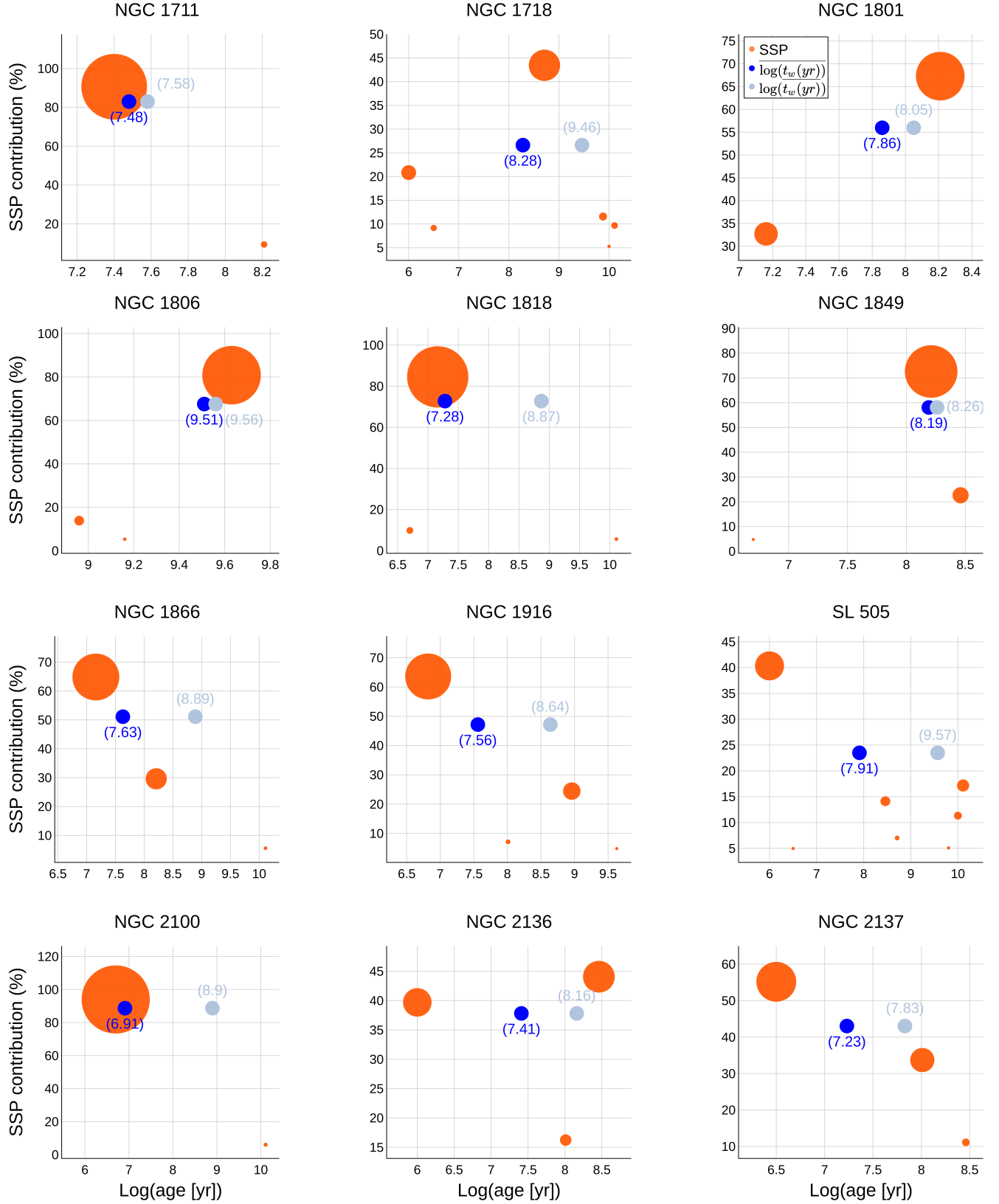


Figure 1. SSP contributions for each star cluster from the STARLIGHT results. From upper left to bottom right: NGC 1711, NGC 1718, NGC 1801, NGC 1806, NGC 1818, NGC 1849, NGC 1866, NGC 1916, SL 505, NGC 2100, NGC 2136, and NGC 2137. In orange the SSP, in blue and light blue are the weighted average age, $\log(t_w(\text{yr}))$, and the log of weighted average age, $\log(t_w(\text{yr}))$, respectively. The size of the orange circles means the contribution rate of each SSP.

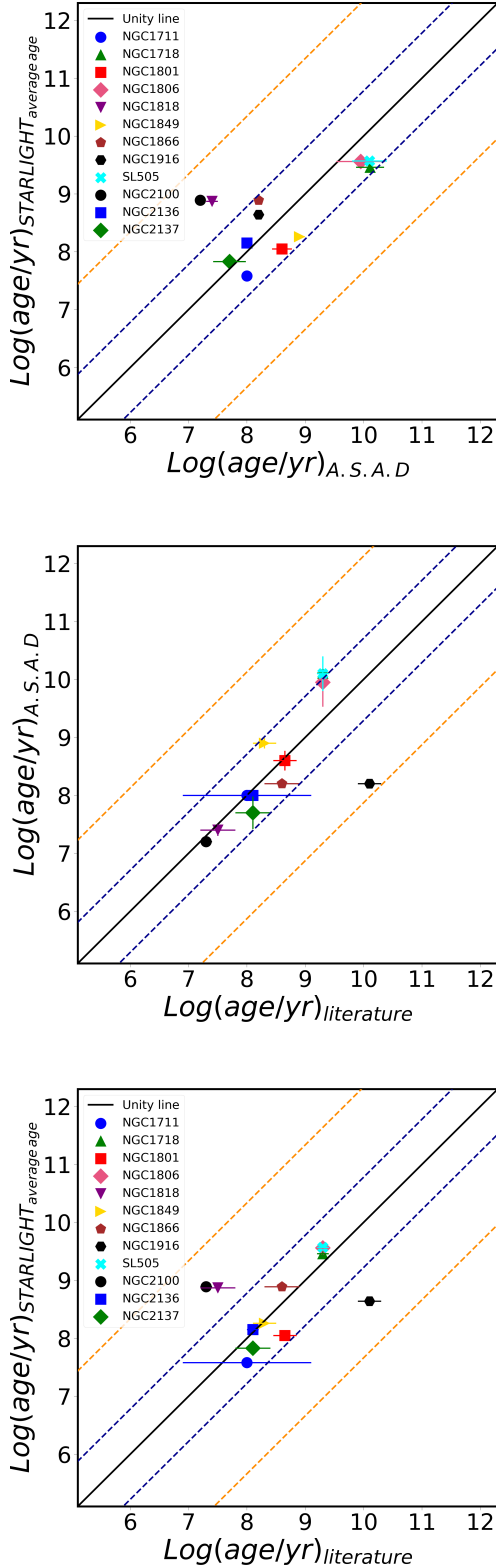


Figure 2. Correlation between A.S.A.D and STARLIGHT age values obtained in this work (top), literature and A.S.A.D (middle) and STARLIGHT (bottom). Errors bars are also indicated. The blue line is the $\pm 1\sigma$ shift and the orange line is the $\pm 3\sigma$ shift.

obtained when using $\log(\overline{t_w(\text{yr})})$ in Figure 2. These results are also shown in Table 2 where column (2) is the weighted average of $\log(\text{age yr}^{-1})$ and column (3) presents the logarithm

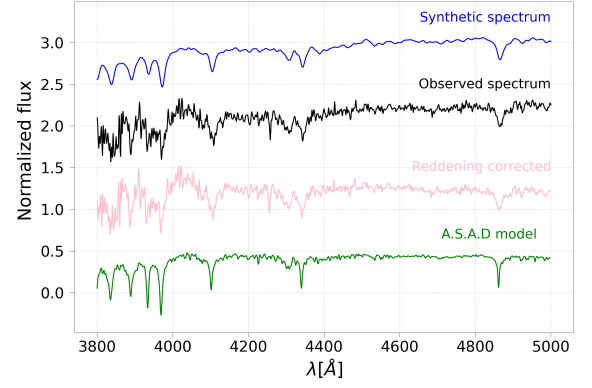


Figure 3. The observed and reddening-corrected (with $E(B - V) = 0.22$) spectra of NGC 1718, in black and pink, respectively, along with the best matching models. A.S.A.D model, with one SSP, in green, and STARLIGHT synthetic spectrum as combination of 6 SSPs, in blue.

of the average age (yr). In this work, we adopt the ages obtained with $\log(\overline{t_w(\text{yr})})$.

Figures Appendix D show the observed integrated spectrum and the best matching model. The results of A.S.A.D are shown on the left side and the results of STARLIGHT are shown on the right side. We define $\overline{\Delta}$ as the mean value of $R_\lambda = |O_\lambda - M_\lambda|$ where the fluxes are normalized and unreddened, with $\overline{\Delta}$ values a measure for the quality of fits. The values are presented in Table 2 and in each residual plot. In general, the residuals of the observed spectrum and the best matching models chosen by each of the two tools are less than 5% in STARLIGHT and 11% in A.S.A.D with the exception of NGC 1806 which is the cluster with the value highest $\overline{\Delta}$ due to its low-S/N ratio (the lowest in our sample). The fitting with STARLIGHT is better because it is based on a combination of different percentage contributions of SSPs. We also note that the spectra with A.S.A.D program are narrower than those from STARLIGHT because according to Equation (1), STARLIGHT fitting applies a default Gaussian convolution to match the spectra. This convolution also plays a role in minimizing the continua mismatch seen in the fits obtained with A.S.A.D. Additionally, although age and reddening are not physically related, they both affect the continuum shape. In the case of NGC 2100, we note that the two tools estimate different reddening values to count for the continuum of the spectrum. The observed and reddening-corrected (with $E(B - V) = 0.22$) spectra of NGC 1718, in black and pink, respectively, along with the best matching models are shown in Figure 3.

We compare the ages obtained with STARLIGHT versus the ones obtained with A.S.A.D in Figure 2. The top panel of the figure shows that the age estimates by STARLIGHT match those obtained with A.S.A.D within 1σ except for NGC 1818 and NGC 2100, which are the youngest clusters according to the literature color-magnitude diagram (CMD) ages (less than $\log(\text{age yr}^{-1}) = 8$). The middle and bottom panels of the figure show that the age predictions of A.S.A.D are closer to the literature values than those obtained from STARLIGHT. The A.S.A.D ages of 11 clusters are within 1σ from the identity line and for STARLIGHT estimations there are 9 clusters within 1σ . We note that based on the literature ages, NGC 1916 is the oldest cluster in our sample, however the ages estimated by both codes (A.S.A.D and STARLIGHT) are underestimated. As shown in the HST-based CMD in K. A. G. Olsen et al. (1998), NGC 1916 is an ancient globular cluster with a blue horizontal branch comparable to that of M92,

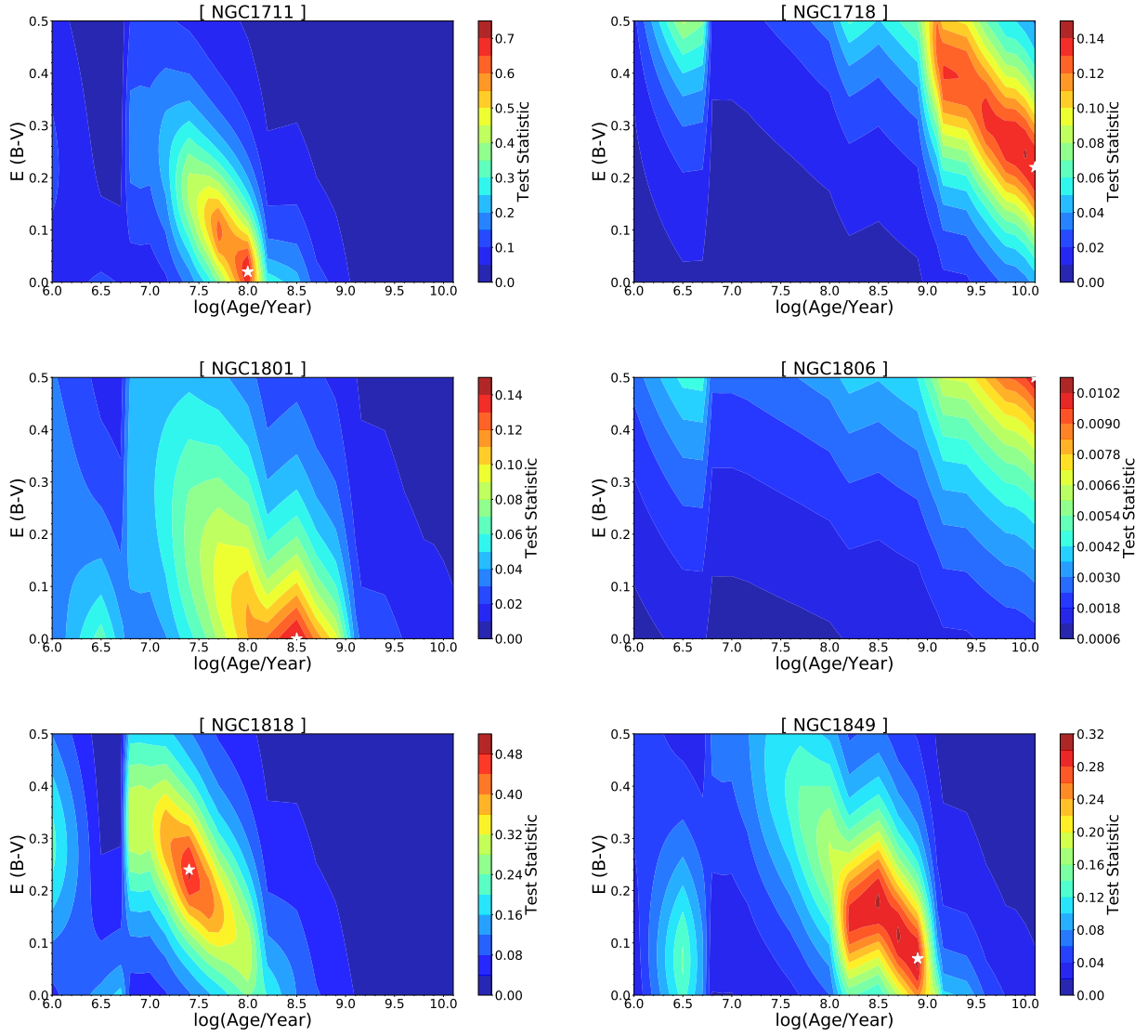


Figure 4. Surface plots of age reddening for each star cluster. From top left to bottom right: NGC 1711, NGC 1718, NGC 1801, NGC 1806, NGC 1818, and NGC 1849.

Table 2
Determined Ages from STARLIGHT and A.S.A.D Codes

Cluster	STARLIGHT			A.S.A.D		Literature	
	$\overline{\log(t_w(\text{yr}))}^{(1)}$	$\log(t_w(\text{yr}))^{(2)}$	$\overline{\Delta} [\%]$	$\log(\text{age yr}^{-1})^{(*)}$	$\overline{\Delta} [\%]$	$\log(\text{age yr}^{-1})$	References
NGC 1711	$7.48^{+0.10}_{-0.09}$	$7.58^{+0.07}_{-0.06}$	1.7	8.00 ± 0.04	2.5	8.00 ± 1.11	Z. Li & X. Liu (2023)
NGC 1718	$8.28^{+0.03}_{-0.04}$	$9.46^{+0.04}_{-0.06}$	4.2	10.11 ± 0.24	5.2	9.3 ± 0.1	A. P. Milone et al. (2023)
NGC 1801	$7.86^{+0.06}_{-0.08}$	$8.05^{+0.03}_{-0.03}$	3.6	8.60 ± 0.17	6.9	8.7 ± 0.2	A. P. Milone et al. (2023)
NGC 1806	$9.51^{+0.18}_{-0.11}$	$9.56^{+0.02}_{-0.02}$	11.6	9.95 ± 0.42	24.9	9.3 ± 0.1	A. P. Milone et al. (2023)
NGC 1818	$7.28^{+0.09}_{-0.22}$	$8.87^{+0.01}_{-0.01}$	1.7	7.40 ± 0.10	2.7	7.5 ± 0.3	A. P. Milone et al. (2023)
NGC 1849	$8.19^{+0.04}_{-0.04}$	$8.26^{+0.02}_{-0.02}$	2.1	8.90 ± 0.09	7.8	8.3 ± 0.2	K. Glatt et al. (2010)
NGC 1866	$7.63^{+0.06}_{-0.08}$	$8.89^{+0.004}_{-0.010}$	2.8	8.20 ± 0.04	3.7	8.6 ± 0.3	A. P. Milone et al. (2023)
NGC 1916	$7.56^{+0.10}_{-0.09}$	$8.64^{+0.01}_{-0.01}$	2.7	8.20 ± 0.05	4.3	10.1 ± 0.2	K. A. G. Olsen et al. (1998)
SL 505	$7.91^{+0.09}_{-0.11}$	$9.57^{+0.03}_{-0.01}$	3.8	10.1 ± 0.30	4.6	9.3 ± 0.1	A. E. Piatti & N. Bastian (2016)
NGC 2100	$6.91^{+0.01}_{-0.01}$	$8.90^{+0.004}_{-0.006}$	1.8	7.20 ± 0.09	3.2	7.3 ± 0.1	F. Niederhofer et al. (2015)
NGC 2136	$7.41^{+0.12}_{-0.12}$	$8.15^{+0.06}_{-0.03}$	3.3	8.00 ± 0.08	3.6	8.1 ± 0.1	F. Niederhofer et al. (2015)
NGC 2137	$7.23^{+0.12}_{-0.27}$	$7.83^{+0.07}_{-0.07}$	2.9	7.70 ± 0.28	6.7	8.1 ± 0.3	K. Glatt et al. (2010)

Note. (1) Logarithm of average log(ages) calculated from Equation (3), (2) Logarithm of average ages calculated using $t_f(\text{yr})$ instead of $\log(t_f(\text{yr}))$ in Equation (3). The precision in the ages derived with STARLIGHT and A.S.A.D were estimated applying R. Asa'd & P. Goudfrooij (2020) method.

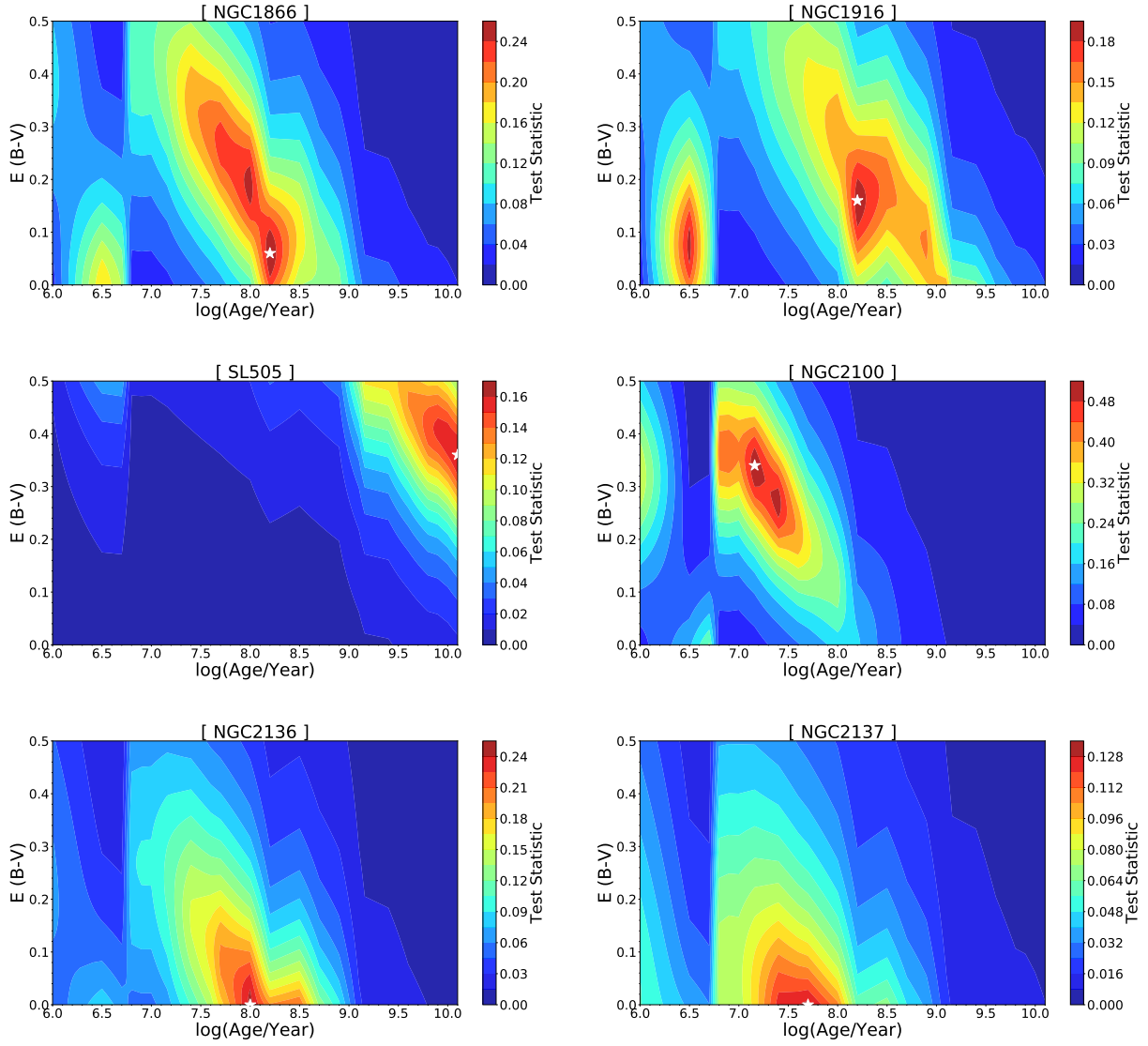


Figure 5. Surface plots of age reddening for each star cluster. From top left to bottom right: NGC 1866, NGC 1916, SL 505, NGC 2100, NGC 2136, and NGC 2137.

indicative of low metallicity. The cluster is located near to the LMC bar, being immersed in a high-field stellar density. Due to the limited spectral resolution of our sample, the age estimation did not match the literature age. R. Asad et al. (2025) showed that this is a limitation of existing models used in the full spectrum fitting technique, as they all underestimate the ages when of old metal-poor clusters. R. S. Asa'd et al. (2017) examined different potential scenarios that could improve the quality of the fit and provided recommendations to improve the theoretical models.

The surface plots of the results obtained with A.S.A.D are shown in Figures 4 and 5. The lowest χ^2 (Equation (2)) values are shown in dark red while the dark blue regions have the highest χ^2 . The white star indicates the location of the minimum χ^2 value obtained by the fitting. This figure reflects the precision of the results. The relatively small dark-red region indicates a precise result; however, NGC 1718, NGC 1849, NGC 1866, NGC 1916, and NGC 2100 show a clear degeneracy of age and reddening.

This figure also reveals the case of NGC 1806, the cluster with the lowest S/N in our sample. R. Asa'd & P. Goudfrooij (2020) showed that the age prediction is strongly affected by the S/N, and that the uncertainties associated with a S/N = 10

for clusters of an age around $\log(\text{age yr}^{-1}) = 9.3$ (which is the literature age of this cluster) are large (± 0.43 dex). The results obtained by each tool are listed in Table 2. The age of the cluster obtained using STARLIGHT, A.S.A.D and from the literature are listed in columns (3), (5), (7), respectively. We aimed to be as uniform as possible when compiling the literature ages. We focused, whenever possible, on recent studies that derive ages from deep HST photometry. The references are listed in column (8). For better visualization, we present them in Figure 6. We analyzed the CMD of each cluster in our sample. According to B. Dirsch et al. (2000), the field of NGC 1711 is rather crowded, A. P. Milone et al. (2023) found very young stars in the fields of NGC 1801 and from a visual inspection of NGC 1849 we detect it as it is the most compact cluster in our sample with less field star contamination. Despite the different levels of background field contamination for these clusters, their age determination is in good agreement with the CMD ages.

5.1. Error Analysis

The error estimates for A.S.A.D ages were obtained using the tables in R. Asa'd & P. Goudfrooij (2020). For consistency, we

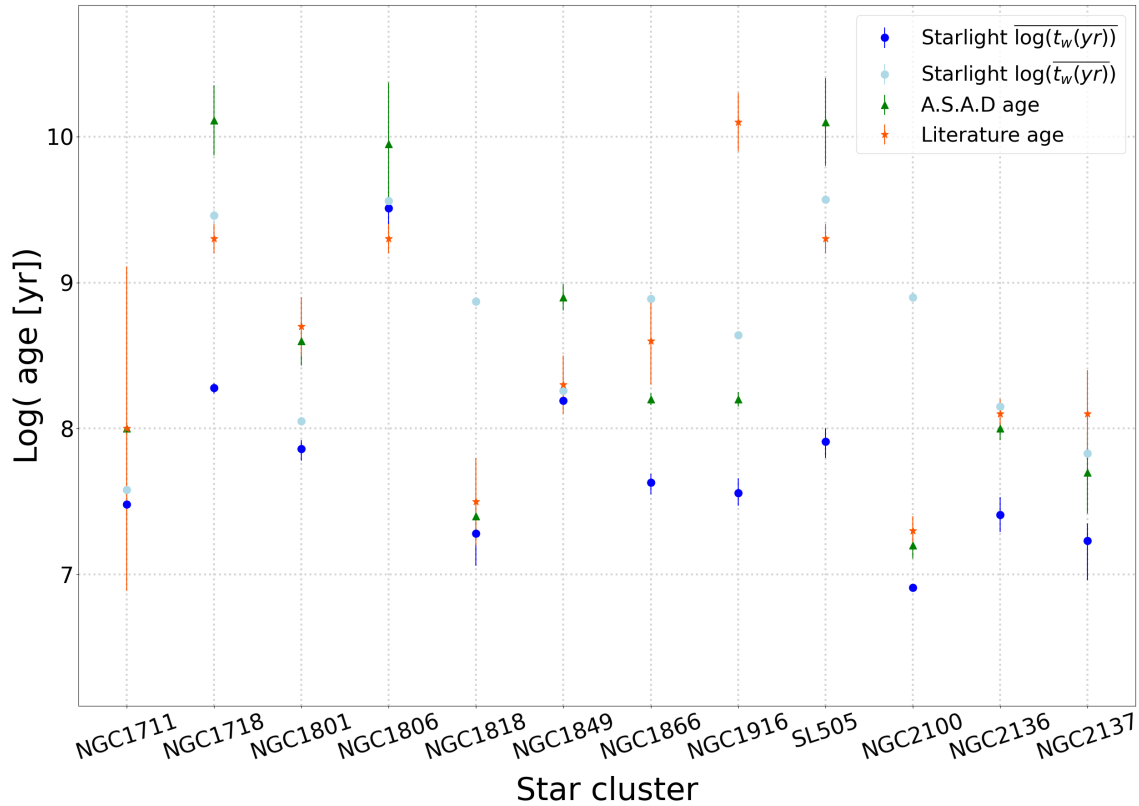


Figure 6. Comparison between A.S.A.D and STARLIGHT age values obtained in this work with literature refereed in Table 2. Errors bars are also indicated.

developed a pipeline to provide the uncertainties associated with the age estimates of STARLIGHT following the same method of R. Asa'd & P. Goudfrooij (2020). We created 23,000 mock clusters based on BC03 models by adding random noise ($10 < S/N < 100$, in steps of 10) for each SSP and performing 100 realizations of each random noise. We estimated the ages of the mock sample using STARLIGHT and determined the error from the statistical parameters employing the SPYCTRAL⁸ library. The errors associated to STARLIGHT ages were determined using the corresponding error from the closest upper and lower ages, respectively. Similar approach is used to obtain the uncertainty in reddening and radial velocity estimates as mentioned in Sections 5.2 and 5.3, respectively.

5.2. Reddening

Although age and reddening are not physically related, they both affect the continuum of the optical spectrum, hence we applied galactic J. A. Cardelli et al. (1989) extinction law with both STARLIGHT and A.S.A.D. There is a technical difference between the two tools related to reddening estimation: A.S.A.D allows the user to choose a range for the applied reddening ($E(B - V)$), while STARLIGHT does not. We used the range $E(B - V) = 0.0-0.5$ in steps of 0.1 with A.S.A.D. We did not apply reddening values greater than 0.5 because they are beyond the expected range for the LMC. (D. Zaritsky et al. 2004; A. V. Ahumada et al. 2019; M. Górski et al. 2020; B. Q. Chen et al. 2022; G. Bhuyan et al. 2024). The results

obtained by each tool are listed in Table 1. Note that the current versions of the programs do not provide uncertainty estimates. Error determination was carried out with 140,760 mock clusters spectra by adding the 51 reddening values described above. The mock sample was based on BC03 models and using a noise range of $10 < S/N < 40$, (in steps of 10) for each SSP and performing 30 realizations of each random noise value. As well as in age errors, we estimated the STARLIGHT errors applying SPYCTRAL tools. The same mock sample was used to obtain the uncertainty in reddening for both codes. STARLIGHT predicted $E(B - V)$ within this range for our sample except for two clusters, SL 505 and NGC 1718. Those also correspond to the clusters that STARLIGHT combined more than 5 SSPs to predict the parameters. On the other hand it is expected that A.S.A.D does not provide an accurate fit for NGC 1806, because it has $S/N = 11$ and hence a bad reddening prediction (see R. Asa'd & P. Goudfrooij 2020 for detailed discussion on the technique's precision as a function of S/N). For NGC 1866 STARLIGHT predicts a value of 0.12 while A.S.A.D predicts 0.06. For the other eight clusters in our sample the difference between STARLIGHT and A.S.A.D predictions is less than 0.15 with 6 of them having a difference of 0.08 or less.

5.3. Radial Velocity

The radial velocity values obtained from each tool are listed in columns (4) and (5) of Table 1. Neither tool provides the uncertainties in radial velocity estimates. The difference between the two values are presented in column (6). In general, the difference is in the range of $\sim 20-50 \text{ km s}^{-1}$ except for the clusters with S/N less than 20 where the difference is larger. For the cluster with the highest S/N the

⁸ SPYCTRAL: astronomical spectral data analyzer is a python package that allows to determine fundamental parameters of compact stellar systems from the analysis of their spectral synthesis and/or templates fitting. Available in: <https://github.com/candelac/Spyspectral>.

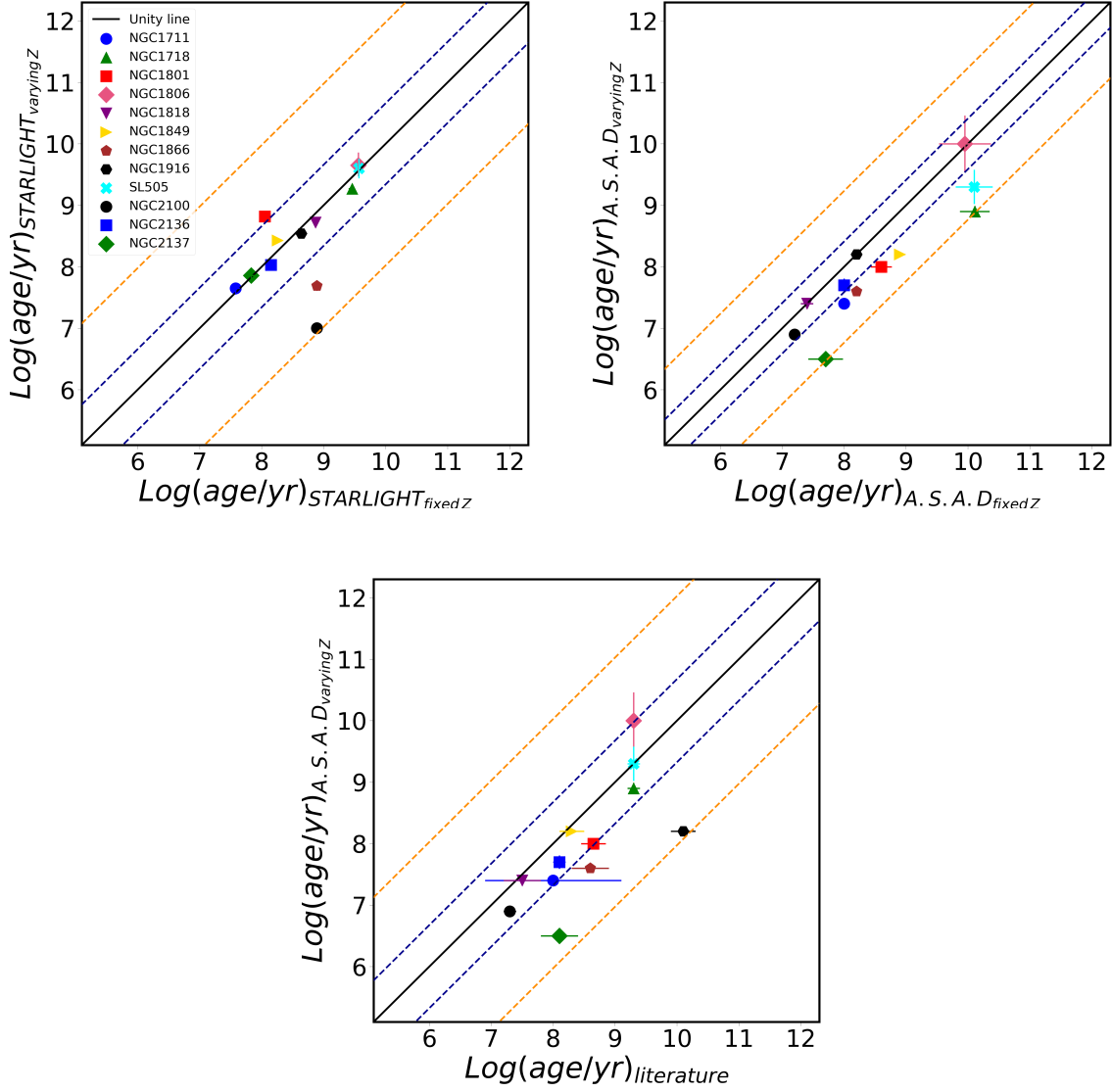


Figure 7. Correlation between A.S.A.D and STARLIGHT age values obtained using a range of metallicities and the fixed $Z = 0.008$. The bottom panel presents A.S.A.D new values vs. literature ones. Errors bars are also indicated. The blue line is the $\pm\sigma$ shift and the orange line is the $\pm3\sigma$ shift.

difference is negligible. For this parameter error determination, we created 19,320 mock spectra, where each of them corresponds to seven different radial velocity values from 100 to 400 km s^{-1} (in step of 50 km s^{-1}) and as well as in reddening values we used $10 < S/N < 40$, (in steps of 10) for each SSP and performing 30 realizations. Both tools give consistent results with the LMC expected values. R. P. van der Marel (2006) determined the observed line-of-sight velocity for LMC to be $262.2 \pm 3.4 \text{ km s}^{-1}$. N. Kallivayalil et al. (2013) estimated a value of $321 \pm 24 \text{ km s}^{-1}$ based on three epochs of HST data and A. E. Piatti et al. (2019) reported a radial velocity of 215 km s^{-1} . More recently, P. Lah et al. (2024) obtained a value of 270 km s^{-1} by measuring the optical emission lines in multiple locations across the LMC using the Australian National University 2.3 m telescope and the Wide-Field Spectrograph. Our radial velocity measurements show that SL 505 has the lowest value. To the best of our knowledge, there are not other studies that estimated the radial velocity of this cluster.

5.4. The Effect of Varying Metallicity

In the previous sections we focused on comparing age estimates between STARLIGHT and A.S.A.D so we excluded any parameters that can contribute to the fitting results. Unlike reddening and radial velocities that are built-in parts of STARLIGHT functionality, metallicity can be kept fixed. In this subsection, we analyze the effect of using a range of metallicities instead of a fixed value by repeating the analysis using a grid of three metallicities: $Z = 0.008$, $Z = 0.004$, and $Z = 0.02$. Figure 7 shows that the age estimates of STARLIGHT are not affected significantly when changing the metallicity, however the results of A.S.A.D are generally underestimated when metallicity is changing as shown on the middle panel. R. Asa'd & P. Goudfrooij (2020) showed that indeed, metallicity measurements with A.S.A.D are not as robust as age estimates. When comparing these new results obtained using A.S.A.D with the literature values, the lower panel of the figure shows that the ages estimates are within 1σ for all clusters (when including uncertainties) except NGC 1916 and NGC 2137.

6. Summary

Using a newly observed sample spectra of LMC star clusters by GMOS-S and BC03 models, we performed for the very first time a systematic comparison between two of the most commonly used tools for getting ages of star clusters from their integrated spectra, STARLIGHT and A.S.A.D. Our results can be summarized in the following points.

(A) The careful analysis of the star clusters for which STARLIGHT uses six and seven SSPs reveals that combining $t_j(\text{yr})$ instead of $\log(t_j(\text{yr}))$ to obtain the weighted average age of the cluster provides results that are more consistent with those from the literature.

(B) There is a good agreement between the ages obtained with STARLIGHT and A.S.A.D. Our clusters are within 1σ from the identity line except for NGC 1818 and NGC 2100, which are the youngest clusters according to literature CMD ages.

(C) Overall, the reddening predictions of STARLIGHT and A.S.A.D match well, except for the cases where A.S.A.D fail due to low S/N or when STARLIGHT predicts values outside the expected range for the LMC, which are the clusters in which more than five SSPs were mixed by STARLIGHT to predict the parameters.

(D) Both tools provide radial velocity estimates consistent with the expected literature value of the LMC. The difference between the results obtained by the two tools depend on the S/N of the observed spectrum. For the cluster with the highest S/N in our sample the difference is negligible, for the other objects the difference is in the range of $\sim 20\text{--}50 \text{ km s}^{-1}$ except for the clusters with S/N less than 20, where the difference is larger.

(E) When varying the metallicity, the age estimates of STARLIGHT are not affected significantly, while the results of A.S.A.D are generally underestimated.

Acknowledgments

We thank the reviewer for the comments that improve our work. This work is based on observations obtained at the international Gemini Observatory, a program of NSF's NOIRLab, which is managed by the Association of Universities for Research in Astronomy (AURA) under a cooperative agreement with the National Science Foundation on behalf of the Gemini Observatory partnership: the National

Science Foundation (United States), National Research Council (Canada), Agencia Nacional de Investigación y Desarrollo (Chile), Ministerio de Ciencia, Tecnología e Innovación (Argentina), Ministério da Ciência, Tecnologia, Inovações e Comunicações (Brazil), and Korea Astronomy and Space Science Institute (Republic of Korea). The Gemini program ID are: GS-2019A-Q-402, GS-2019B-Q-401 and GS-2021B-Q-401. This work is supported by the FRG Grant and the Open Access Program from the American University of Sharjah. This paper represents the opinions of the authors and does not mean to represent the position or opinions of the American University of Sharjah. M.I.T.R. and A.V.A. acknowledge the support by the Consejo de Investigaciones Científicas y Técnicas de la República Argentina (CONICET), the Secretaría de Ciencia y Técnica de la Universidad Nacional de Córdoba (SeCyT) and the Agencia Nacional de Promoción Científica y Tecnológica (PICT 2019-03824). C.G.D. acknowledge "Agencia Nacional de promoción de la investigación, el desarrollo tecnológico y la innovación" through project PICT-2021-GRF-TII-00442, and the support of CONICET through project PIP 11220210100520CO. This research has made use of NASA's Astrophysics Data System Bibliographic Services, and the SIMBAD database, CDS, Strasbourg Astronomical Observatory, France 2000, A&AS, 143, 9, "The SIMBAD astronomical database," Wenger et al. This research has made use of Aladin sky atlas, CDS, Strasbourg Astronomical Observatory, France 2000, A&AS, 143, 33, "The ALADIN interactive sky atlas. A reference tool for identification of astronomical sources," Bonnarel et al. and 2014, ASPC, 485, 277, "Aladin Lite: Embed your Sky in the Browser," Boch et al. and 2022, ASPC, 532, 7, "Aladin Lite v3: Behind the Scenes of a Major Overhaul," Baumann et al.

Appendix A The Star Clusters Sample

Figure 8 presents DSS images for the star clusters sample with 6.5×6.5 sizes. The observed regions are indicated with all slit positions in yellow. Table 3 presents the significance of the atmospheric differential refraction in integrated spectra of each stellar cluster in the sample.

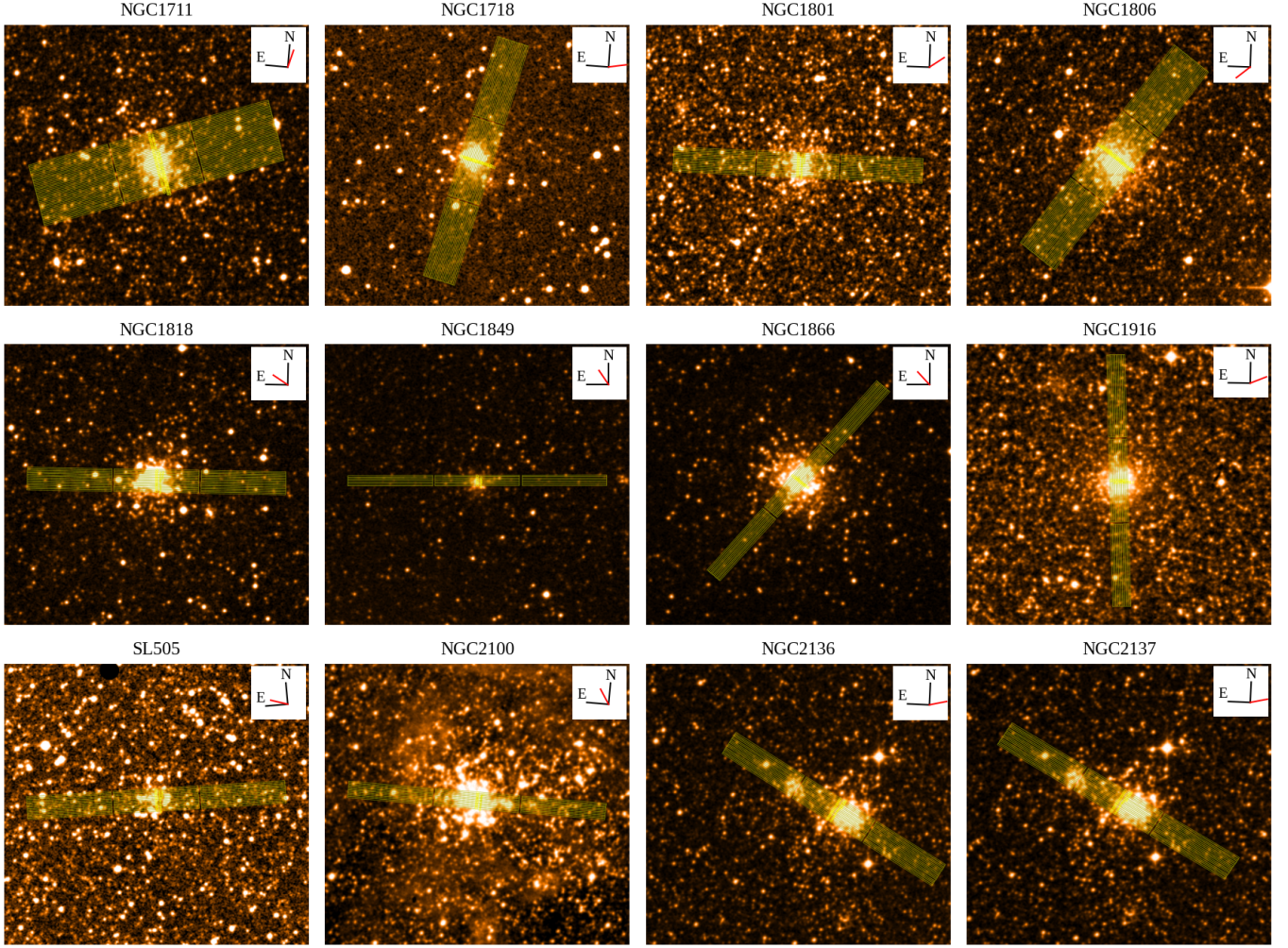


Figure 8. DSS images for the star clusters sample ($6'.5 \times 6'.5$). From upper left to bottom right: NGC 1711, NGC 1718, NGC 1801, NGC 1806, NGC 1818, NGC 1849, NGC 1866, NGC 1916, SL 505, NGC 2100, and NGC 2136 and NGC 2137. The observed regions are indicated in yellow, showing all slit positions (width = $2''.0$ length = $5''.5$). North, east (black), and the zenith (red) direction are indicated in each panel.

Table 3
Significance of the Atmospheric Differential Refraction in Integrated Spectra of Stellar Clusters

Cluster	N^a Offset Positions	Scanned Region Width ^b ($''$)	PA ^c ($^\circ$)	Parallactic Angle ($^\circ$)	Average Airmass	ADR ^d ($''$)	ADR-to-Scan Width ^e (%)
NGC 1711	41	82	290	345.63	1.49	0.71	0.87
NGC 1718	22	44	166	280.82	1.41	0.62	1.41
NGC 1801	16	32	90	304.61	1.40	0.62	1.94
NGC 1806	29	58	144	129.11	1.36	0.58	1.00
NGC 1818	15	30	90	56.50	1.42	0.62	2.07
NGC 1849	7	14	270	33.33	1.28	0.53	3.79
NGC 1866	11	22	138	41.81	1.31	0.53	2.41
NGC 1916	11	22	0	293.51	1.49	0.71	3.23
SL 505	15	30	90	71.59	1.66	0.84	2.80
NGC 2100	11	22	90	32.36	1.34	0.58	2.64
NGC 2136	17	34	60	283.78	1.59	0.80	2.35
NGC 2137	17	34	60	283.78	1.59	0.80	2.35

Notes.

^a Number of offset positions observed per cluster.

^b Width of the total scanned region calculated as $N \times$ slit width ($2''$).

^c Position Angle of the slit.

^d Atmospheric Differential Refraction from A. V. Filippenko (1982).

^e Maximum percentage of the scanned region width affected by ADR for the extreme case of a slit orientation perpendicular to the parallactic angle.

Appendix B

Spectral Synthesis Results from STARLIGHT

The SSPs contributions obtained from the spectral synthesis performed with STARLIGHT for each star cluster are presented

in Table 4. Figure 1 shows all those relations between each SSP contribution with the weighted average of log(ages) for all the sample.

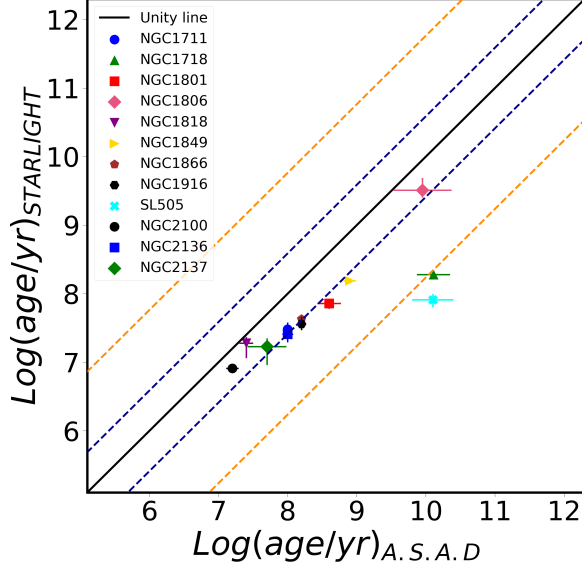
Table 4
SSPs Contributions from STARLIGHT with Fixed Z Value

Cluster	Weighted Average Log (age yr ⁻¹)	SSP Age	SSP Contribution (%)
NGC 1711	$7.48^{+0.10}_{-0.09}$	7.40	90.6
		8.21	9.4
NGC 1718	$8.28^{+0.03}_{-0.04}$	8.71	43.4
		6.00	20.8
		9.88	11.6
		10.11	9.7
		6.50	9.2
NGC 1801	$7.86^{+0.06}_{-0.08}$	10.00	5.3
NGC 1806	$9.51^{+0.18}_{-0.11}$	8.21	67.3
		7.16	32.7
NGC 1818	$7.28^{+0.09}_{-0.22}$	9.63	80.8
		8.96	13.9
		9.16	5.3
NGC 1849	8.19 ± 0.04	7.16	84.5
		6.7	9.8
		10.11	5.6
NGC 1866	$7.63^{+0.06}_{-0.08}$	8.21	72.6
		8.46	22.6
		6.7	4.8
NGC 1916	$7.56^{+0.10}_{-0.09}$	7.16	64.8
		8.21	29.6
		10.11	5.6
SL 505	$7.91^{+0.09}_{-0.11}$	6.82	63.6
		8.96	24.5
		8.01	7.1
		9.63	4.8
NGC 2100	6.91 ± 0.01		
		6.0	40.3
		10.11	17.2
		8.46	14.1
		10	11.3
NGC 2136	7.41 ± 0.12	8.71	7
		9.8	5.1
		6.5	5
NGC 2137	$7.23^{+0.12}_{-0.27}$	6.7	94
		10.11	6
NGC 2137		8.46	44.1
		6.0	39.7
		8.01	16.2
NGC 2137		6.5	55.2
		8.01	33.7
		8.46	11.1

Appendix C

Ages Correlations Obtained from A.S.A.D and STARLIGHT

Ages comparisons obtained with STARLIGHT versus the ones from A.S.A.D. STARLIGHT ages were obtained from Equation (3) that make the average of $\log(\text{ages})$. The correlation between literature and STARLIGHT ages using a range of metallicities and fixed ones. Errors bars are also indicated. The lines are showing $\pm\sigma$ shift.



Appendix D

Residual Plots Obtained from A.S.A.D and STARLIGHT

This appendix presents the residual plots in Figures 9–12, obtained from A.S.A.D run and STARLIGHT. The observed spectrum and the selected model in the best fit is showed for each cluster. We also present the residual flux at the bottom and it is also indicated the $\bar{\Delta}$ defined as the mean value of $R_\lambda = |O_\lambda - M_\lambda|$ as a measure for the quality of fits.

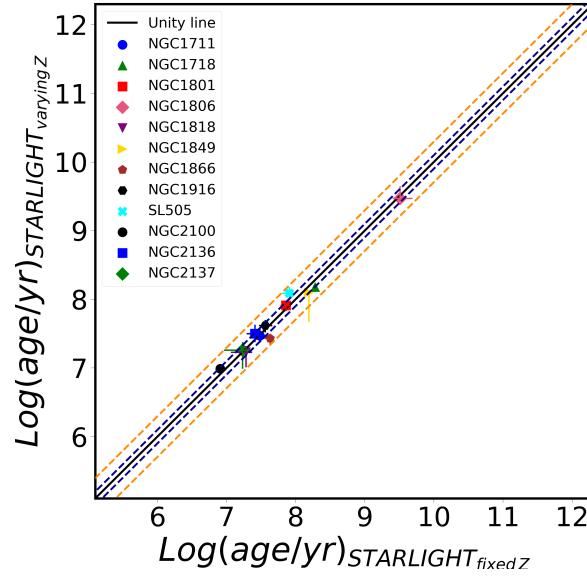
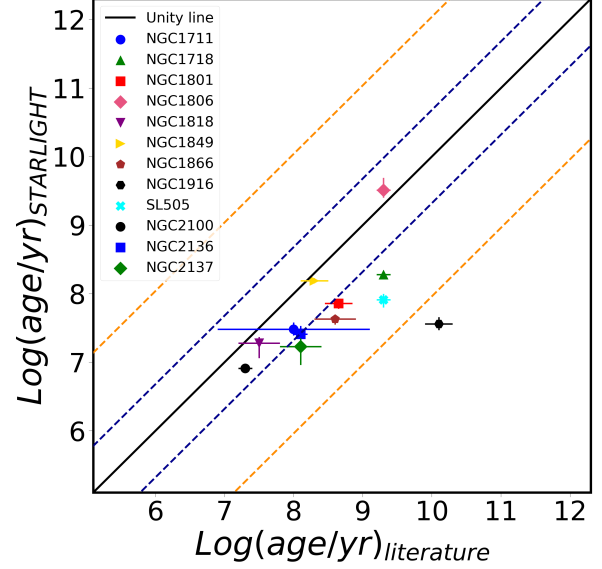


Figure 9. Correlation between A.S.A.D and STARLIGHT age values obtained in this work (top), literature and STARLIGHT (middle), using a range of metallicities and fixed ones. Errors bars are also indicated. The blue line is the $\pm\sigma$ shift and the orange line is the $\pm3\sigma$ shift.

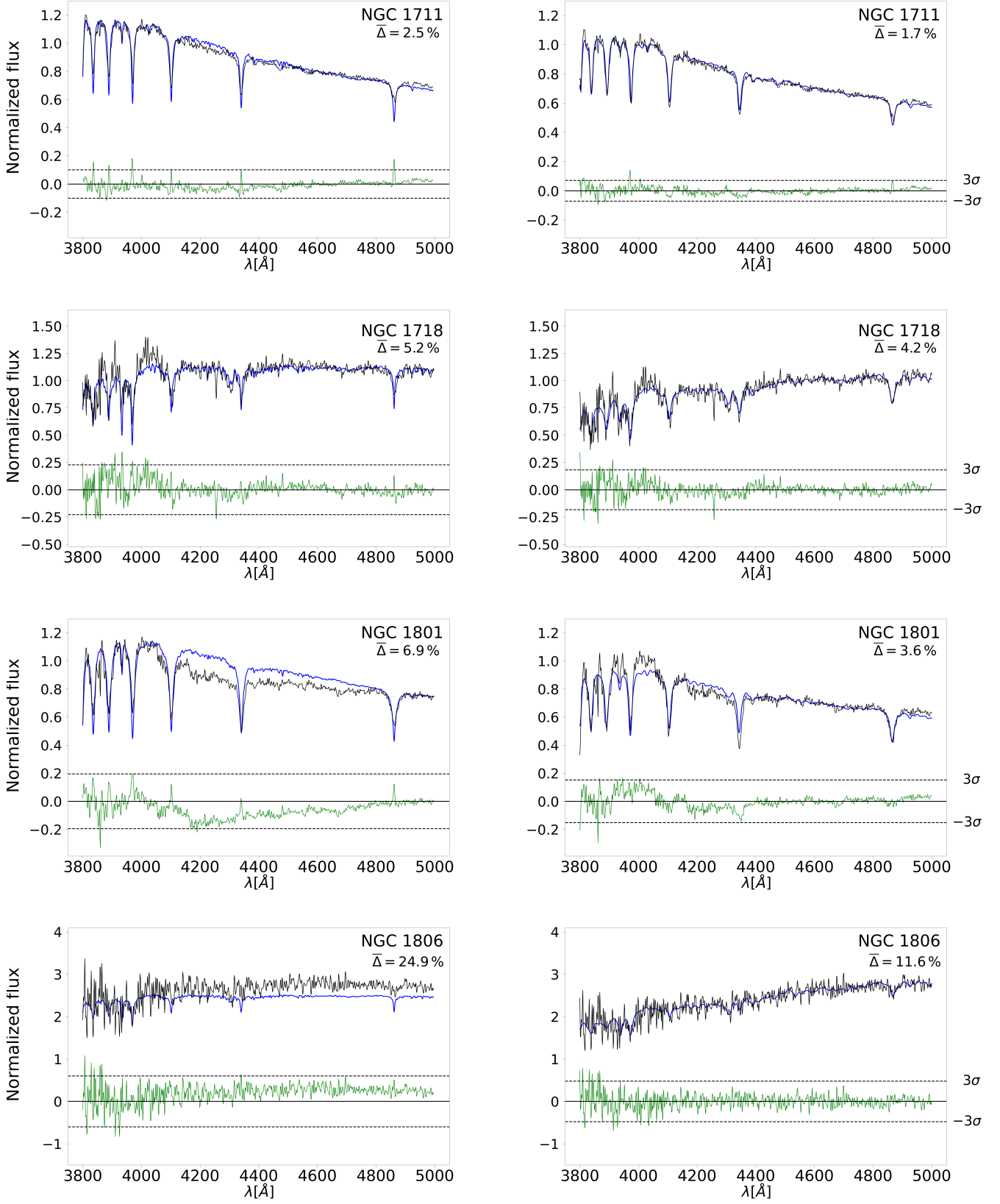


Figure 10. Normalized reddening-corrected spectrum using A.S.A.D. (left panels) and observed normalized spectrum using STARLIGHT (right panels) in black, and the best matching models fit in blue. The residual flux is presented in green. The dotted lines are at $\pm 3\sigma$. The percentage mean ($\bar{\Delta}$) is indicated for each cluster.

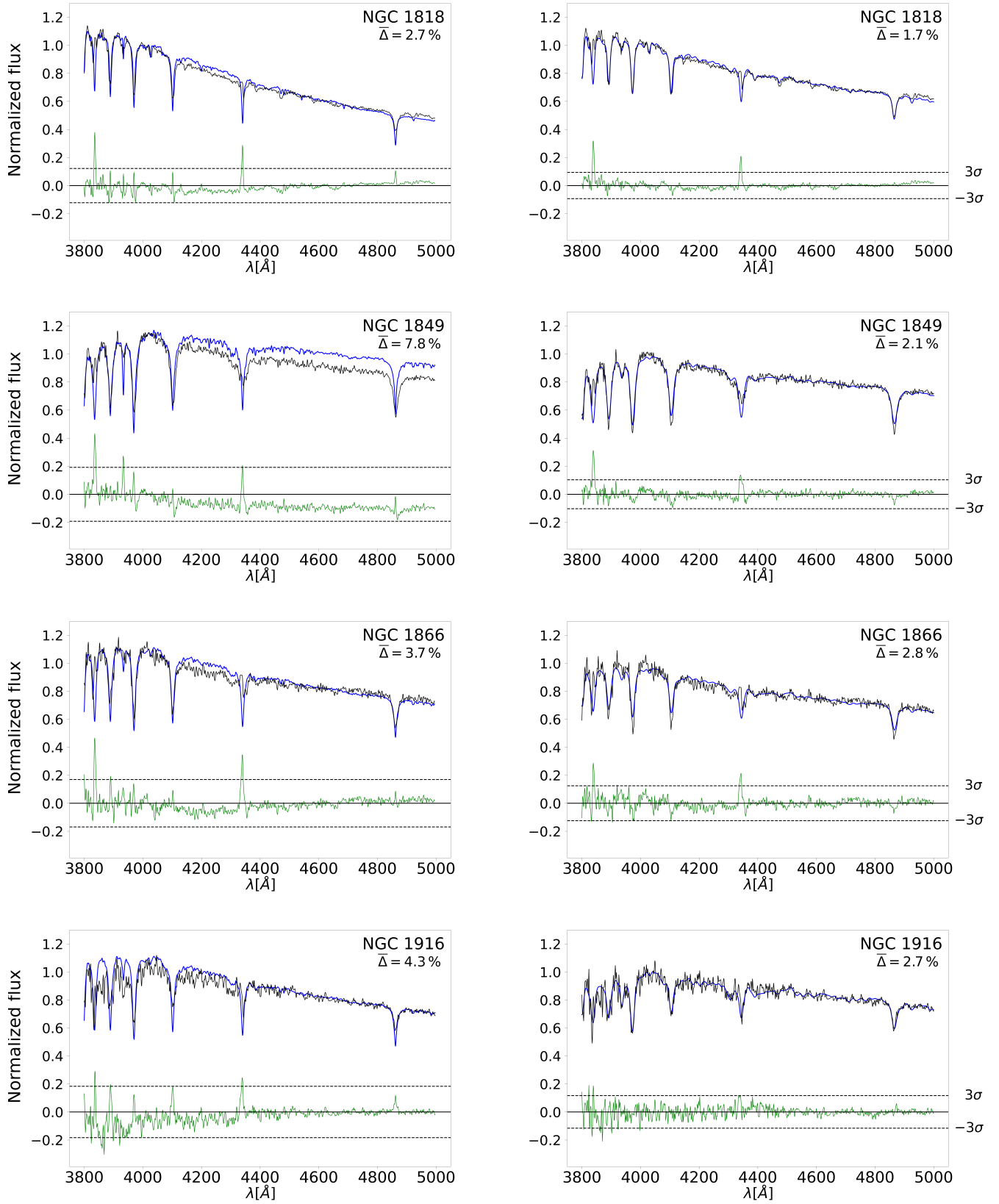


Figure 11. Continued from Figure 10.

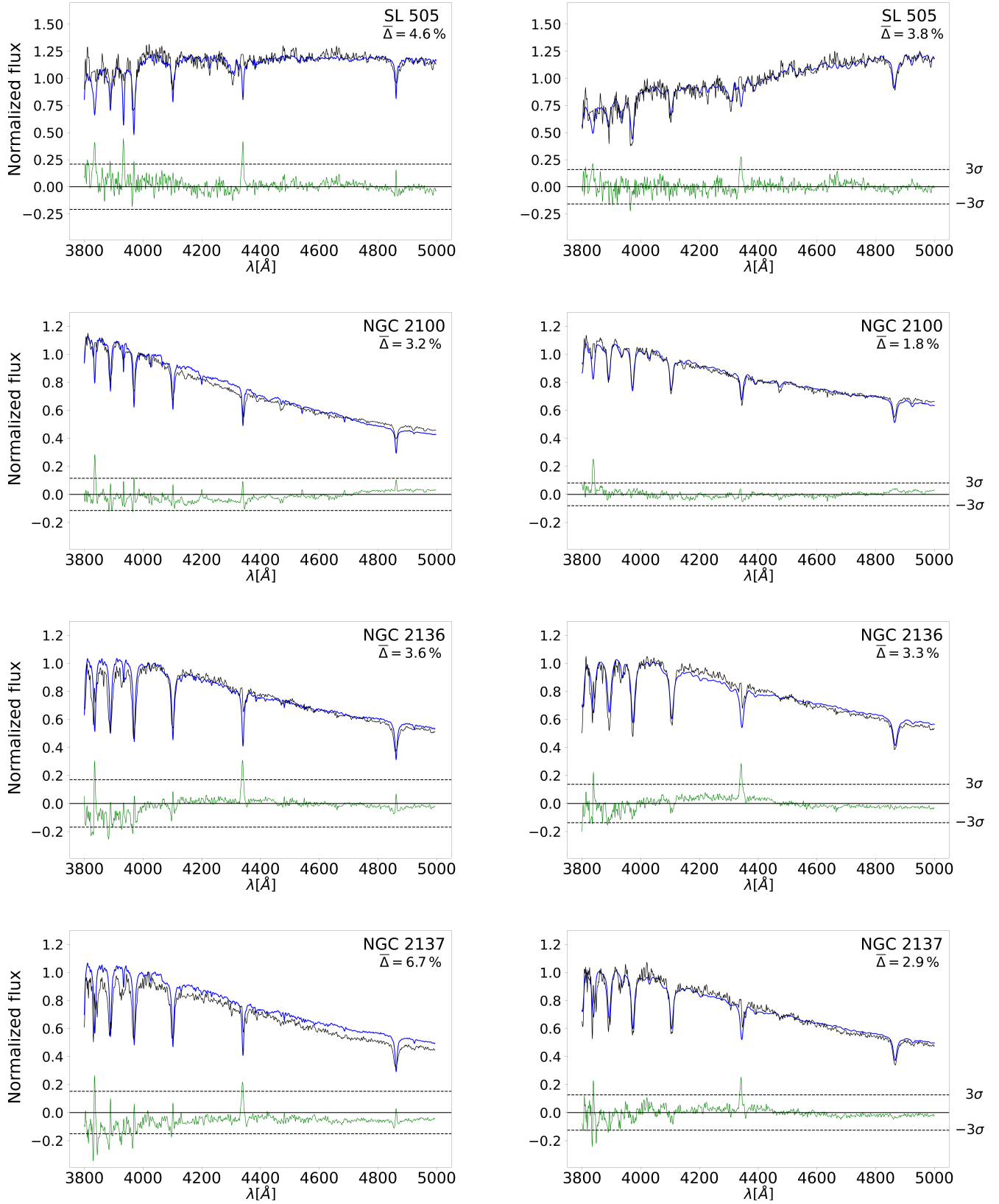






Figure 12. Continued from Figure 10.

ORCID iDs

Martina I. Tapia-Reina  <https://orcid.org/0009-0002-5075-2502>
 Randa Asa'd  <https://orcid.org/0000-0003-4861-6624>
 Andrea V. Ahumada  <https://orcid.org/0000-0002-9233-4475>
 Carlos Gonzalo Díaz  <https://orcid.org/0000-0001-5146-1358>

References

- Adamo, A., Zeidler, P., Kruijssen, J. M. D., et al. 2020, *SSRv*, **216**, 69
 Ahumada, A. V., Vega-Neme, L. R., Clariá, J. J., & Minniti, J. H. 2019, *PASP*, **131**, 024101
 Asad, R., Coelho, P. R. T., John, J. M., et al. 2025, arXiv:2504.03194
 Asa'd, R., & Goudfrooij, P. 2020, *MNRAS*, **498**, 2814
 Asa'd, R., Goudfrooij, P., & As'ad, A. M. 2022, *MNRAS*, **512**, 2014
 Asa'd, R., Goudfrooij, P., As'ad, A. M., et al. 2021, *MNRAS*, **505**, 979
 Asa'd, R. S. 2014, *MNRAS*, **445**, 1679
 Asa'd, R. S., Hanson, M., & Ahumada, A. V. 2013, *PASP*, **125**, 1304
 Asa'd, R. S., Vazdekis, A., Cerviño, M., et al. 2017, *MNRAS*, **471**, 3599
 Bastian, N., Usher, C., Kamann, S., et al. 2019, *MNRAS*, **489**, L80
 Benítez-Llambay, A., Clariá, J. J., & Piatti, A. E. 2012, *PASP*, **124**, 173
 Berek, S. C., Reina-Campos, M., Eadie, G., & Sills, A. 2023, *MNRAS*, **525**, 1902
 Bhuyan, G., Deb, S., Kanbur, S. M., et al. 2024, *MNRAS*, **527**, 8671
 Bruzual, G., & Charlot, S. 2003, *MNRAS*, **344**, 1000
 Cardelli, J. A., Clayton, G. C., & Mathis, J. S. 1989, *ApJ*, **345**, 245
 Chabrier, G. 2003, *PASP*, **115**, 763
 Chen, B. Q., Guo, H. L., Gao, J., et al. 2022, *MNRAS*, **511**, 1317
 Chilingarian, I., Prugniel, P., Sil'chenko, O., & Koleva, M. 2007, in IAU Symp. 241, *Stellar Populations as Building Blocks of Galaxies*, ed. A. Vazdekis & R. Peletier (Cambridge: Cambridge Univ. Press), 175
 Chilingarian, I. V., & Asa'd, R. 2018, *ApJ*, **858**, 63
 Choudhury, S., Subramaniam, A., & Cole, A. A. 2016, *MNRAS*, **455**, 1855
 Cid Fernandes, R., & González Delgado, R. M. 2010, *MNRAS*, **403**, 780
 Cid Fernandes, R., Mateus, A., Sodré, L., Stasińska, G., & Gomes, J. M. 2005, *MNRAS*, **358**, 363
 Clariá, J., Ahumada, A., Bica, E., Pavani, D., & Parisi, M. 2017, *NewA*, **56**, 71
 Colucci, J. E., Bernstein, R. A., Cameron, S. A., & McWilliam, A. 2012, *ApJ*, **746**, 29
 Colucci, J. E., Bernstein, R. A., & McWilliam, A. 2017, *ApJ*, **834**, 105
 Dias, B., Coelho, P., Barbuy, B., Kerber, L., & Idiart, T. 2010, *A&A*, **520**, A85
 Dirsch, B., Richtler, T., Gieren, W. P., & Hilker, M. 2000, *A&A*, **360**, 133
 Filippenko, A. V. 1982, *PASP*, **94**, 715
 Glatt, K., Grebel, E. K., & Koch, A. 2010, *A&A*, **517**, A50
 Gonçalves, G., Coelho, P., Schiavon, R., & Usher, C. 2020, *MNRAS*, **499**, 2327
 Górski, M., Zgierski, B., Pietrzyński, G., et al. 2020, *ApJ*, **889**, 179
 Goudfrooij, P., & Asa'd, R. S. 2021, *MNRAS*, **501**, 440
 Graves, G. J., & Schiavon, R. P. 2008, *ApJS*, **177**, 446
 Greggio, L., & Renzini, A. 2011, *Stellar Populations. A User Guide from Low to High Redshift* (New York: Wiley-VCH-Verlag)
 Kallivayalil, N., van der Marel, R. P., Besla, G., Anderson, J., & Alcock, C. 2013, *ApJ*, **764**, 161
 Lah, P., Colless, M., D'Eugenio, F., Groves, B., & Gelfand, J. D. 2024, *MNRAS*, **529**, 2611
 Li, Z., & Liu, X. 2023, *MNRAS*, **525**, 827
 Marigo, P., Girardi, L., Bressan, A., et al. 2008, *A&A*, **482**, 883
 Milone, A. P., Cordoni, G., Marino, A. F., et al. 2023, *A&A*, **672**, A161
 Moura, T. C., Trevisan, M., Barbuy, B., & Rossi, S. 2019, *ApJ*, **885**, 28
 Niederhofer, F., Hilker, M., Bastian, N., & Silva-Villa, E. 2015, *A&A*, **575**, A62
 Olsen, K. A. G., Hodge, P. W., Mateo, M., et al. 1998, *MNRAS*, **300**, 665
 Palma, T., Ahumada, A. V., Clariá, J. J., Santos, J. F. C., Jr., & Bica, E. 2008, *AcA*, **58**, 359
 Piatti, A. E., & Bastian, N. 2016, *MNRAS*, **463**, 1632
 Piatti, A. E., Salinas, R., & Grebel, E. K. 2019, *MNRAS*, **482**, 980
 Puzia, T. H., Kissler-Patig, M., & Goudfrooij, P. 2006, *ApJ*, **648**, 383
 Puzia, T. H., Kissler-Patig, M., Thomas, D., et al. 2005, *A&A*, **439**, 997
 Sakari, C. M., Shetrone, M. D., McWilliam, A., & Wallerstein, G. 2021, *MNRAS*, **502**, 5745
 Santos, J. F. C., Jr., Clariá, J. J., Ahumada, A. V., et al. 2006, *A&A*, **448**, 1023
 Schiavon, R. P., Rose, J. A., Courteau, S., & MacArthur, L. A. 2005, *ApJS*, **160**, 163
 Simondi-Romero, F., Ahumada, A., & Vega-Neme, L. 2022, *BAAA*, **63**, 115
 van der Marel, R. P. 2006, in *The Local Group as an Astrophysical Laboratory*, ed. M. Livio & T. M. Brown, Vol. 17 (Cambridge: Cambridge Univ. Press), 47
 van Dokkum, P. G. 2001, *PASP*, **113**, 1420
 Zaritsky, D., Harris, J., Thompson, I. B., & Grebel, E. K. 2004, *AJ*, **128**, 1606